University of New Hampshire
University of New Hampshire Scholars' Repository

Physics Scholarship   Physics

8-1-1998

Coronal mass ejections, magnetic clouds, and relativistic magnetospheric electron events: ISTP

D. N. Baker

T. I. Pulkkinen

X. Li

S. G. Kanekal

J. B. Blake

See next page for additional authors

Follow this and additional works at: https://scholars.unh.edu/physics_facpub

Part of the Physics Commons

Authors

D. N. Baker, T. I. Pulkkinen, X. Li, S. G. Kanekal, J. B. Blake, R. S. Selesnick, M. G. Henderson, G. D. Reeves, Harlan E. Spence, and G. Rostoker

Coronal mass ejections, magnetic clouds, and relativistic magnetospheric electron events: ISTP

D. N. Baker,[1] T. I. Pulkkinen,[1,2] X. Li,[1] S. G. Kanekal,[3] J. B. Blake,[4] R. S. Selesnick,[4] M. G. Henderson,[5] G. D. Reeves,[5] H. E. Spence,[6] and G. Rostoker[7]

Abstract. The role of high-speed solar wind streams in driving relativistic electron acceleration within the Earth's magnetosphere during solar activity minimum conditions has been well documented. The rising phase of the new solar activity cycle (cycle 23) commenced in 1996, and there have recently been a number of coronal mass ejections (CMEs) and related "magnetic clouds" at 1 AU. As these CME/cloud systems interact with the Earth's magnetosphere, some events produce substantial enhancements in the magnetospheric energetic particle population while others do not. This paper compares and contrasts relativistic electron signatures observed by the POLAR, SAMPEX, Highly Elliptical Orbit, and geostationary orbit spacecraft during two magnetic cloud events: May 27-29, 1996, and January 10-11, 1997. Sequences were observed in each case in which the interplanetary magnetic field was first strongly southward and then rotated northward. In both cases, there were large solar wind density enhancements toward the end of the cloud passage at 1 AU. Strong energetic electron acceleration was observed in the January event, but not in the May event. The relative geoeffectiveness for these two cases is assessed, and it is concluded that large induced electric fields ($\partial B/\partial t$) caused in situ acceleration of electrons throughout the outer radiation zone during the January 1997 event.

1. Introduction

The Sun is increasingly likely to expel large clouds of material (called coronal mass ejections (CMEs)) during the peak of its 11-year activity cycle. These can move outward from the Sun with speeds in excess of 1000 km/s [*Kahler*, 1992]. The shock waves preceding such plasma structures can accelerate interplanetary particles to high energies, sometimes up to several hundred million electron volts (MeV). If the shock waves and "magnetic clouds" associated with CMEs strike the Earth's magnetosphere, they can initiate major geomagnetic storms that can disrupt power systems, degrade communication links, and increase the probability of anomalous behavior of operational spacecraft on which our society increasingly relies [e.g., *Baker*, 1996; see also http://www-istp.gsfc.nasa.gov/istp.newsletter.html/]. The appreciation of CMEs as the agents of such substantial

[1]Laboratory for Atmospheric and Space Physics, University of Colorado, Boulder.

[2]Permanently at Finnish Meteorological Institute, Helsinki.

[3]NASA Goddard Space Flight Center, Greenbelt, Maryland.

[4]The Aerospace Corp., Space and Environment Technology Center, Los Angeles, California.

[5]Los Alamos National Laboratory, Los Alamos, new Mexico.

[6]Center for Space Physics, Boston University, Boston, Massachusetts.

[7]Department of Physics, University of Alberta, Edmonton, Canada.

solar disturbances of geospace has come about in the past few years: This "paradigm" shift has had a far-reaching impact on how we think about solar-terrestrial relationships [e.g., *Gosling*, 1993].

The International Solar-Terrestrial Physics (ISTP) program has put into place a large array of spacecraft and ground facilities for studying the space environment [e.g., *Acuña et al.*, 1995]. The observational resources offered by ISTP attained a rather complete configuration with the launch of POLAR in February 1996. The Sun reached its minimum sunspot activity in mid-1996 and began to exhibit characteristics of the new activity cycle (E. Hildner, private communication, 1997). Consequently, several CMEs have been observed on the Sun which subsequently reached the Earth's vicinity. In this paper, we examine two such CMEs and we consider the "geoeffectiveness" of their interaction with Earth's magnetosphere. In particular, the efficiency of relativistic electron acceleration in the outer magnetosphere due to the CMEs is reported here. Such acceleration is assessed in the context of another mode of solar wind-magnetosphere coupling which has been shown to be quite effective at electron acceleration, namely, high-speed solar wind stream events [*Baker et al.*, 1994; *Blake et al.*, 1997; *Li et al.*, 1997a].

2. Interplanetary Drivers of Geospace Disturbances

2.1 Recurrent Geomagnetic Storms

High-speed solar wind streams originate in solar coronal holes [*Feldman et al.*, 1978]. Generally, transequatorial coronal holes are well developed in the declining phase of the solar cycle (rather than right at sunspot minimum). Long-term observations in the outer magnetosphere (at $L{\sim}6.6$)

have demonstrated that energetic electron fluxes are strongly modulated by solar wind streams [*Baker et al.*, 1986]. Lower-energy ($\lesssim$ 300 keV) particle fluxes track the solar wind variations quite closely and, as illustrated by Figure 1, appear to be the direct product of magnetospheric substorm activity [see *Baker et al.*, 1978; *Nishida*, 1983, and references therein]. Higher-energy ($\gtrsim$ 300 keV) particle fluxes in the outer trapping regions (L=4~7) are also modulated by the solar wind streams, but peak fluxes are typically delayed relative to substorm-related enhancements (see Figure 1). The highest-energy magnetospheric electrons show strong recurrence tendencies at the 27-day rotation period of the Sun [*Williams*, 1966; *Paulikas and Blake*, 1979] and are closely related to "recurrent" geomagnetic storms [*Baker et al.*, 1997a].

On the basis of recent observations, it is concluded that even during near-minimum solar conditions (sunspot minimum) there are discernible coronal source regions and resultant solar wind streams which can produce intense magnetospheric particle acceleration. Plate 1 summarizes electron counting rate data for the 2-6 MeV energy range using the Solar, Anomalous, and Magnetospheric Particle Explorer (SAMPEX). It shows that long-lasting electron events in late-March 1996 and again in April 1996 were closely related in time to high-speed ($V \geq$ 600 km/s) solar wind streams [*Baker et al.*, 1997a]. In May, June, and July the solar wind speed was quite low, and the radiation belts became very weak. From August and into October 1996 there were again numerous high-speed stream events. By late 1996, however, the magnetosphere had become rather quiet, and during November and December 1996 there was only one brief instance of solar wind speed above ~600 km/s. Notably, the period of mid- to late-January 1997 produced another large electron counting rate enhancement in the SAMPEX data which will be discussed here.
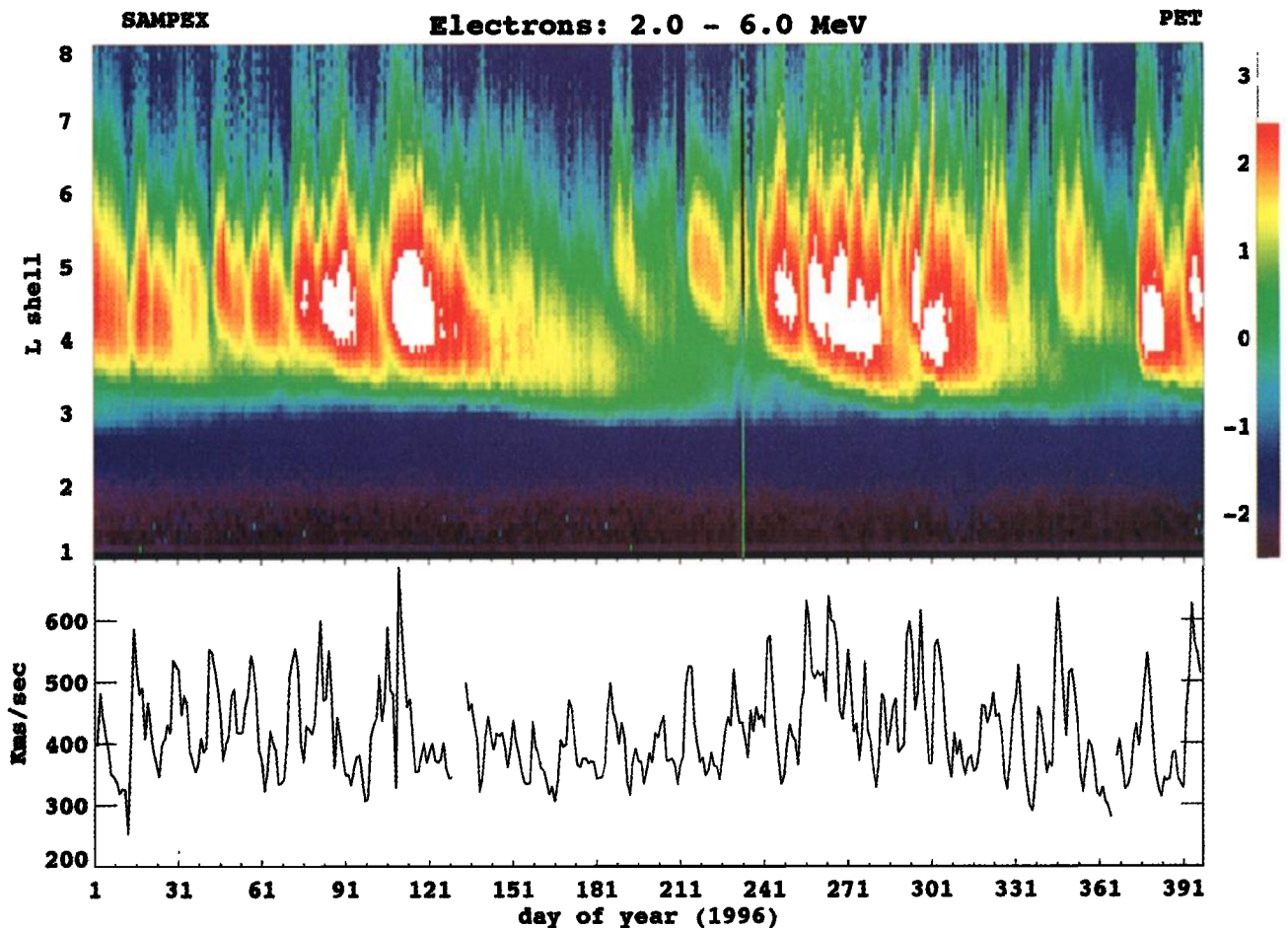
2.2 High-Energy Electron Acceleration

Observations as in Plate 1 indicate that relativistic electrons increase in measured counting rate, often by a factor of 10 or more, throughout much of the outer magnetosphere on a timescale of order 1 day even during rather weak recurrent geomagnetic storm activity [*Baker et al.*, 1997a; *Blake et al.*, 1997]. Abrupt count rate enhancements occur in the outer magnetosphere, as well as at low L shells, deep within the magnetospheric cavity. Geomagnetic activity is controlled by the solar wind speed and by the interplanetary magnetic field (IMF) orientation [e.g., *Nishida*, 1983]. The combination of high V_{SW} and strong (southward) IMF drives intense substorm activity. This produces copious quantities of energetic electrons in the energy range 30~300 keV [*Baker et al.*, 1978]. As a second step in the electron acceleration sequence, *Baker et al.* [1997b] noted that the highest-energy electrons and the hardest spectra occur some days after the substorm activity peaks. Thus the outer zone magnetospheric electrons behave in a quite coherent way. This coherence is manifested spatially, temporally, and spectrally. On the basis of previous observations, an acceleration sequence can be summarized as in Figure 2. The solid line shows the spectrally soft enhancement which is a prompt response to an increase of V_{SW}. The dashed line shows the spectral hardening as the solar wind speed decreases. The intense relativistic electron population appears some days after the leading edge of the solar wind stream has passed the Earth. Thus the highest relativistic electron flux is seen throughout the outer zone when V_{SW} is decreasing.

Although substorm disturbances provide an important seed population of energetic electrons needed for major relativistic electron events [*Baker et al.*, 1997b], it apparently is the further extraction of energy from the solar wind stream as it buffets the magnetosphere that ultimately produces the higher-energy electron population [see *Blake et al.*, 1997]. The mechanism that takes the lower-energy seed population and converts many of these subrelativistic electrons to highly relativistic particles has not yet been fully understood [see *Li et al.*, 1997b).

2.3 CME-Generated Storms

In contrast to recurrent storms, large nonrecurrent geomagnetic storms develop at Earth as a result of such aperiodic solar events as the CMEs discussed above which are normally associated with eruptive prominences and other solar disturbances. It is sometimes, but certainly not always, found that the leading edges of CMEs are moving outward from the Sun at a speed much higher than that of the normal solar wind [see *Burlaga*, 1995]. Thus such fast CMEs can move rapidly through the ambient plasma of the heliosphere. Their outward motion can lead to great distortion of the IMF and, given a sufficiently high relative speed, CMEs can be drivers for strong interplanetary shock waves. The field compression and draping ahead of the magnetic clouds caused by CMEs often leads to stronger than normal magnetic fields at the leading edge of the structure and the high plasma flow velocity can produce a geomagnetic storm and particle acceleration due to a large magnetospheric field

Figure 1. A schematic (adapted from Hruska and Hruska [1989]) showing a typical high-speed solar wind (V) profile (solid curve) and the associated interplanetary magnetic field (IMF) profile (dashed curve). The combination of high B and large V at the leading edge of the stream can drive strong substorm activity (especially if the z component of the IMF is negative). In the time period of declining V, there is strong acceleration of relativistic magnetospheric electrons.

Plate 1. (top) A color-coded plot of 2-6 MeV electron counting rates as a function of the magnetic-shell (L) parameter. Data are shown as the logarithm of counts/s (as shown by the color bar) from day 1 of 1996 to the end of January 1997). (bottom) The hourly average of the solar wind speed measured by the SWE investigation onboard the WIND spacecraft. A general association of high energy electrons for $3 \leq L \leq 7$ with high solar wind speed ($V \geq 500$ km/s) is demonstrated.

compression and distortion. CME events observed recently have not had particularly high speeds. However, when compared to recurrent solar wind stream events that have characterized the solar minimum, these recent CME/cloud events provide a contrasting view of how magnetospheric electrons may be rapidly accelerated.

3. CME/Magnetic Cloud Observations

Data are presented here for two magnetic cloud (CME-related) events. The interplanetary measurements and the magnetospheric responses will be compared and contrasted using a wide range of data sets. Despite the apparent similarity of the two cases, their effectiveness in accelerating high-energy electrons is found to be strikingly different.

3.1 Case 1: May 27-29, 1996

Figure 3a shows interplanetary data from the WIND spacecraft (data courtesy of K. Ogilvie and R. Lepping) for May 26 through May 29, 1996. WIND was upstream of the Earth's bow shock throughout and provided a continuous record of the solar wind [*Ogilvie et al.*, 1995] and IMF

[*Lepping et al.*, 1995] properties. The top panel of Figure 3a shows the IMF magnitude (B) in nanoteslas, while the second panel from the top shows the north-south IMF component (B_z) for the same period. There was a distinctive increase in B at ~1400 UT on May 27. At this same time, the B_z component went abruptly and strongly negative. For the subsequent 40 hours or so, the IMF magnitude remained high and the B_z component slowly and systematically rotated toward being strongly northward. By ~1200 UT on May 29, following several strong field fluctuations, the value of B returned to low values ($B \leq 5$ nT) and B_z returned to values near zero. The period May 27 (1400 UT) to May 29 (1200 UT) was identified as a magnetic cloud interval (see *Burlaga* [1995] for a general discussion of magnetic clouds).

The solar wind speed (V) and number density (n) shown, respectively, in the two bottom panels of Figure 3a demonstrate that the bulk speed of the cloud plasma was not any higher than the ambient solar wind (~400 km/s), but the density was relatively high (>10 cm^{-3}). The value of n increased progressively throughout the cloud passage and reached a peak value of ~60 cm^{-3} near the end of the cloud interval.
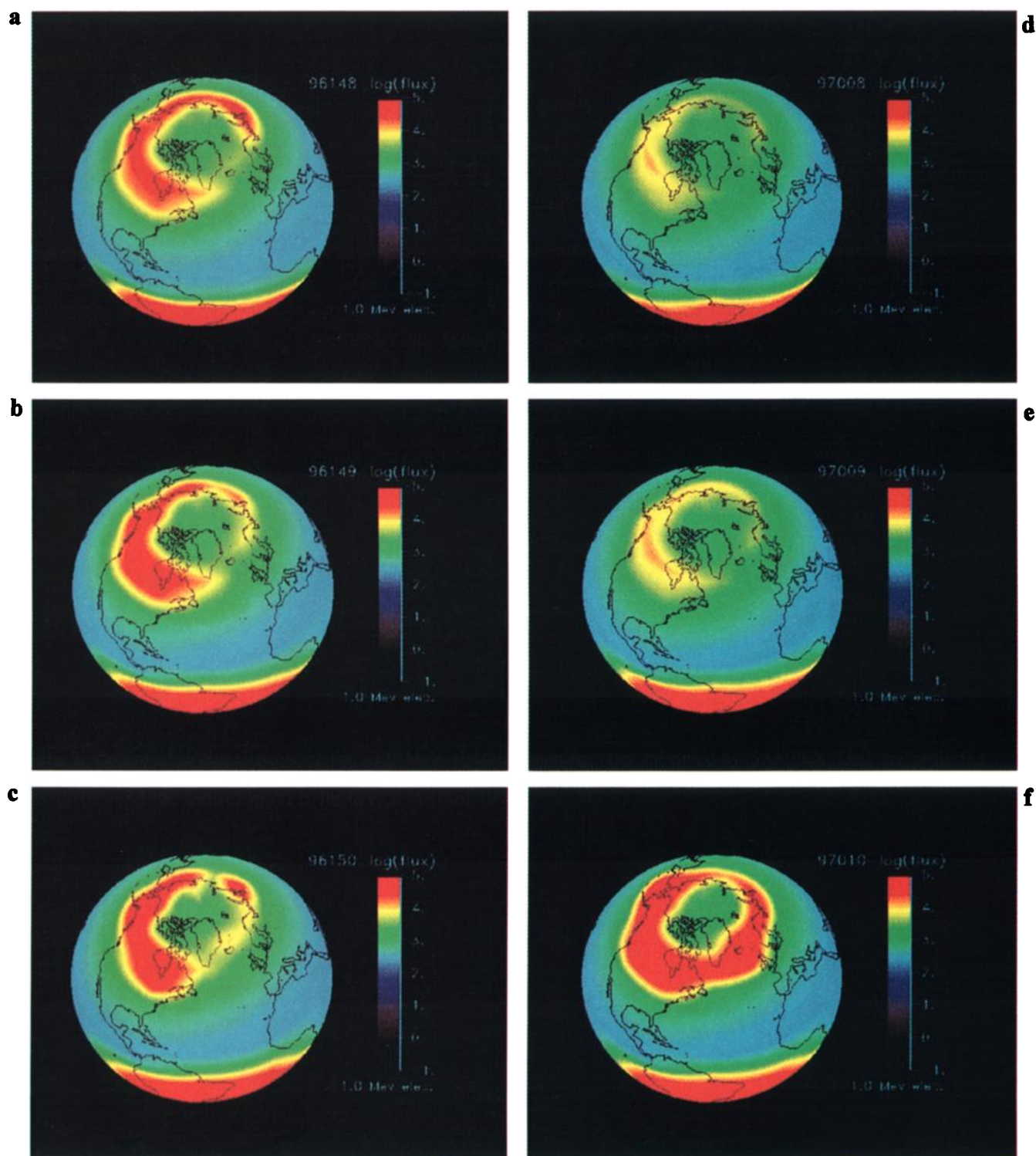
Plate 2. Color-coded global maps of the >1.0 MeV electron counting rates measured by SAMPEX. Data are projected onto a global geographic grid and the log of counts/s are color-coded as shown by the color bars. (a) to (c) cover days 148 to 150 of 1996 and (d) to (f) cover days 8 to 10 of 1997.
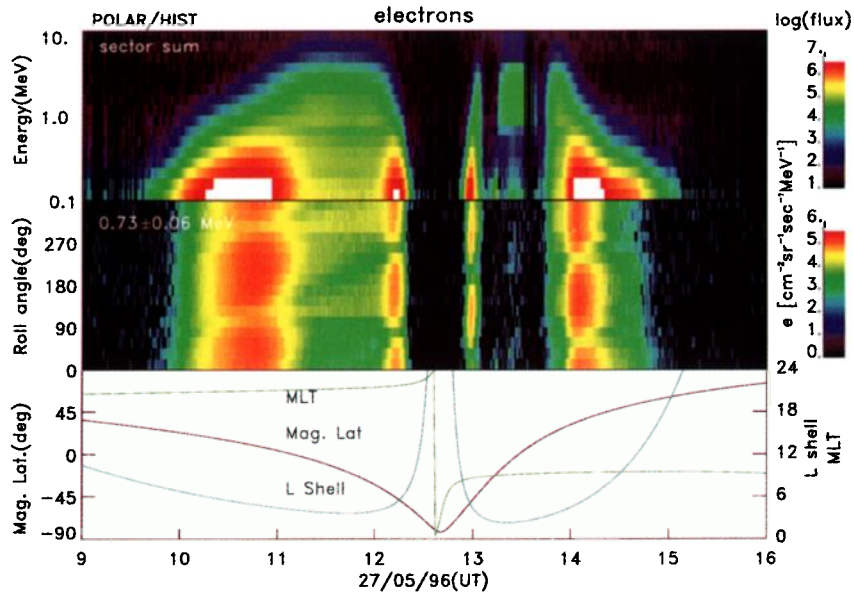
Plate 3. Color spectrograms and orbital information for the POLAR/HIST instrument for 0900-1600 UT on May 27, 1996. The middle panel shows angle-time information for electrons with E = 0.73 ± 0.06 MeV. The top panel shows an energy-time spectrogram for the same period. The bottom panel shows the magnetic local time (MLT), magnetic latitude (MLat), and L value for the POLAR spacecraft.

There are several available indicators of the strength of solar wind energy input to the magnetosphere. Among these indicators is the energy "coupling parameter", $\varepsilon[=VB^2\ell_o^2 \sin^4(\Theta/2)]$ devised by *Perreault and Akasofu* [1978]. In this formula, ℓ_o =7 R_E (a constant) and Θ is the clock angle made between the IMF and the Earth's magnetic dipole. Another measure of geomagnetic response is provided by vari-

ous magnetic indices such as *AU, AL*, and *Dst* [see *Mayaud*, 1980]. Yet a further measure of magnetospheric response to solar wind driving is the level and variability of energetic particles at geostationary orbit [e.g., *Baker et al.*, 1978]. Figure 4a shows all of these parameters for May 26-29, 1996.

The top panel of Figure 4a demonstrates that on May 26
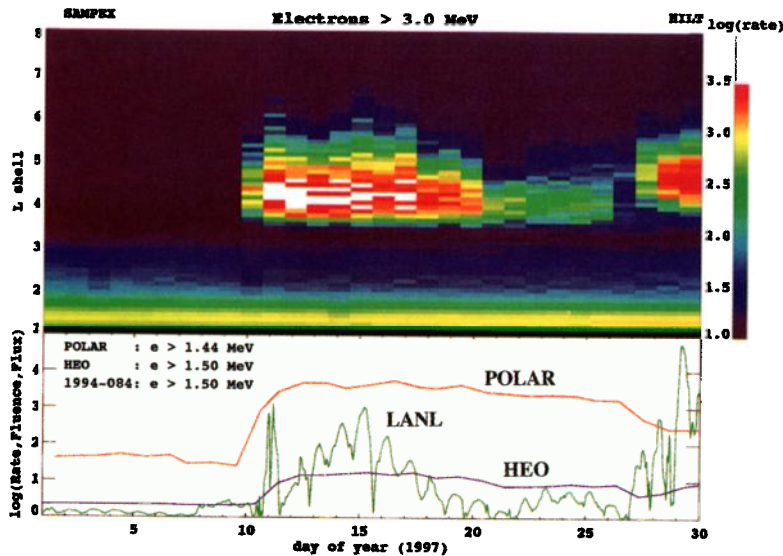
Plate 4. (top) A comparison of SAMPEX counting rates (counts/s) and several other spacecraft for high energy electrons measured during January 1997. (bottom) POLAR/HIST, HEO, and LANL geostationary data. The POLAR data are for electrons with energies $E>1.44$ MeV and are shown as counts/s. The HEO data ($E>1.5$ MeV) are presented in terms of fluence (rads/day). The LANL data are for energies $E>1.5$ MeV and are presented at electrons/(cm^2-s-sr). All data sets tend to track one another showing the global coherence of relativistic electron events with a rapid flux enhancement on January 10.
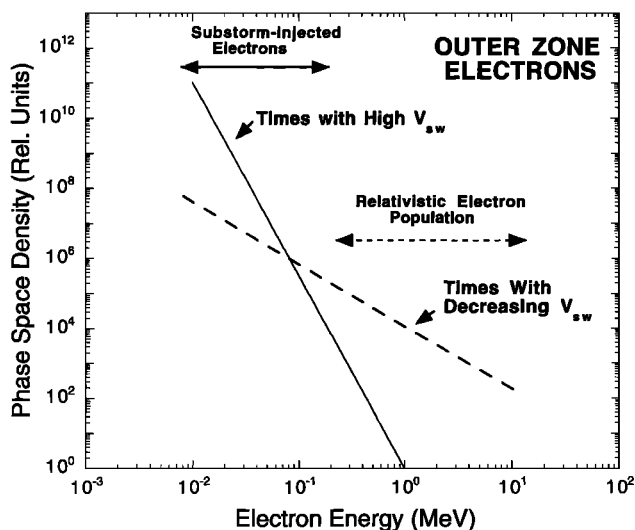
Figure 2. A schematic representation of the electron phase space density variations seen during recurrent solar wind stream events. The outer zone energetic electron spectrum systematically shifts during the time that solar wind speed peaks and then subsides. Substorms initially produce many relatively low energy electrons, some of which subsequently get boosted to higher energies.

and 27, ε was well below the level (ε=10^{11}W) of typical substorm activity [*Perreault and Akasofu*, 1978] prior to the arrival of the magnetic cloud. With the cloud's arrival, ε rose abruptly to ~3×10^{11}W and stayed above 10^{11}W until

~1600 UT on May 28. During this period, especially on May 27, the CANOPUS provisional *AU* and *AL* parameters [see *Rostoker et al.*, 1995b] showed substantial activity. (Note that occasional data gaps occur in the CANOPUS *AL* or *AU* indices when high-confidence values are not available). Substorm electrojet activity of several hundred nanotesla levels was frequently recorded. The third panel from the top presents the preliminary *Dst* data for this period and shows only a weak ring current development (*Dst* ≈ -30 nT) when ε was at its maximum value. Finally, the lower two panels of Figure 4a show the medium energy electron (50 ≤ *E* ≤ 225 keV) and proton (50 ≤ *E* ≤ 250 keV) fluxes measured onboard S/C 1994-084 at geostationary orbit [see *Reeves et al.*, 1998, and references therein]. Several relatively weak and energy-dispersive flux enhancements (both electron and proton) were seen at geostationary orbit during the cloud passage.

An important question about interplanetary disturbances, as discussed in the prior section, is how efficiently the disturbance accelerates high-energy magnetospheric particles. Figure 5a shows the daily-average fluxes of 2-6 MeV electrons measured by SAMPEX at low-Earth orbit. The data have been sorted according to *L* value and are plotted for the broad interval extending from day 140 (May 19) through day 159 (June 7) of 1996. The magnetic cloud interval (days 147-150) is delineated by the vertical dashed lines. It is not evident at this temporal resolution that the magnetic cloud had any discernible impact on the flux levels of these multi-MeV electrons for 2 ≤ *L* ≤ 5. A slight modulation of the flux might have been present near *L*=6.

A more global representation of SAMPEX data during the cloud interval is shown in Plate 2a-2c. These daily plots of
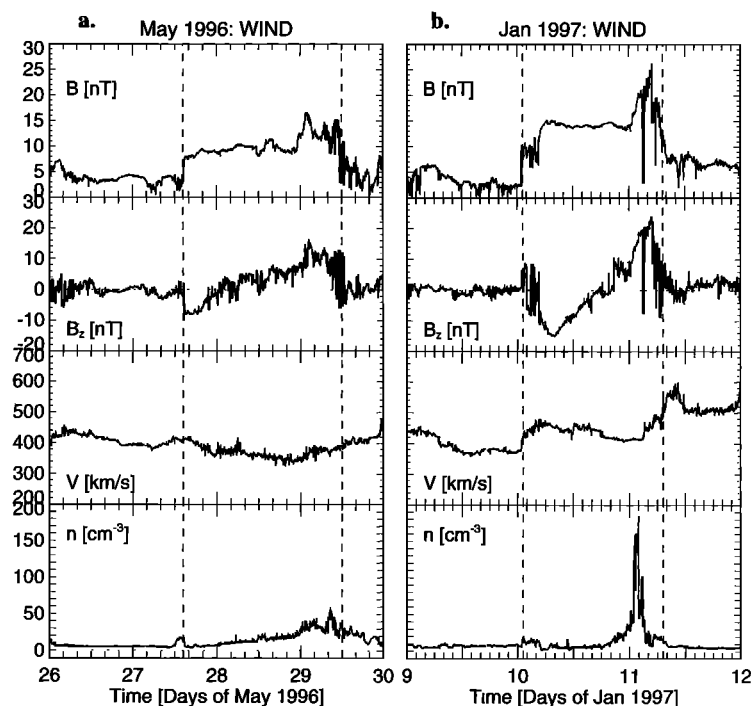
Figure 3. (a) The IMF magnitude (*B*) and north-south (*B_z*) component along with the solar wind speed (*V*) and density (*n*) for May 26-29, 1996. The "magnetic cloud" interval extended from 1400 UT on May 27 to 1200 UT on May 29. (b) The same quantities for the period January 9-11, 1997. The cloud interval in this case was 0100 on January 10 to ~0800 UT on January 11.
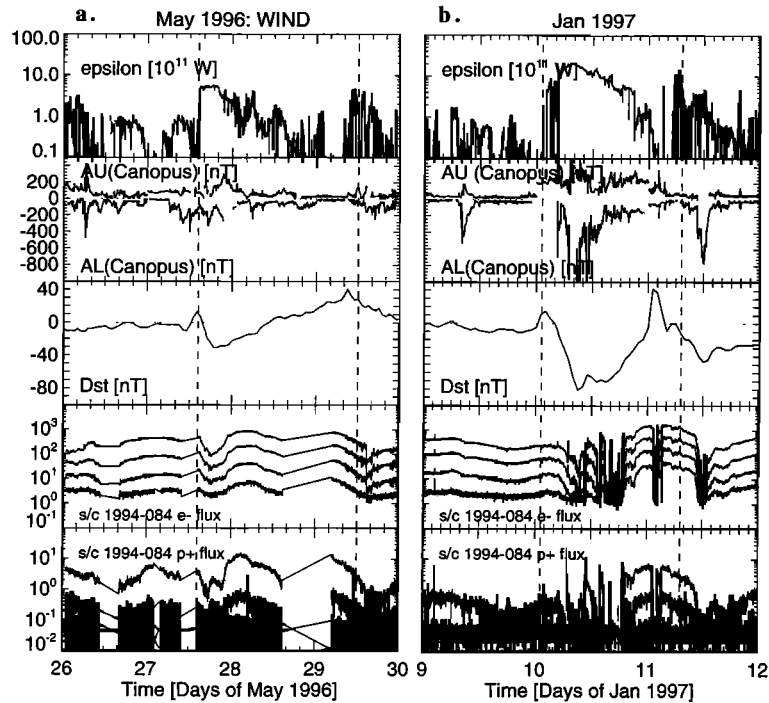
Figure 4. Solar wind energy input (ε) parameter and magnetospheric responses (AU, AL, Dst, and geostationary orbit energetic particle fluxes) for the two magnetic cloud periods: (a) May 26-29, 1996 and (b) January 9-11, 1997. The AU and AL values are computed only from the CANOPUS chain of magnetometers. The electron fluxes are in the energy ranges 50-75, 75-105, 105-150, and 150-225 keV. Proton channels cover similar energies. The particle fluxes are in units of $(cm^2\text{-}s\text{-}sr\text{-}keV)^{-1}$.

the electron counting rate for $E>1$ MeV are projected as a global map for days 148, 149, and 150 (May 27-29). Very little difference is evident from one day to the next, therefore substantiating the point also made in Figure 5a that this magnetic cloud was not effective at producing multi-MeV electrons.

The POLAR spacecraft, launched in February 1996, made repeated cuts through the radiation belts on its ~17.5-hour, high-inclination orbit. During late May 1996, the orbit plane was in the 0900-2100 LT meridian and POLAR cut through L values ≥ 2.5. Plate 3 shows a High-Sensitivity Telescope (HIST) color spectrogram for the period 0900 to 1600 UT on May 27, 1996. HIST covers the electron energy range ~0.1 to ~10 MeV and is part of the POLAR Comprehensive Energetic Particle Pitch Angle Distribution (CEPPAD) investigation [Blake et al., 1995]. The top panel of Plate 3 is a color-coded energy-time spectrogram. The flux of electrons is indicated by the color bar to the right of the panel. The second panel of Plate 3 shows "roll-angle" versus time where fluxes are again color-coded, in this case for energies at 0.73 ± 0.06 MeV. The particle distribution is plotted for angles that are reckoned from the ecliptic-plane (ascending node) as POLAR executes its "cartwheel" rotation in the orbital plane. The lowest panel in Plate 3 shows L, LT, and magnetic latitude (as labeled) for the POLAR orbit during this time.
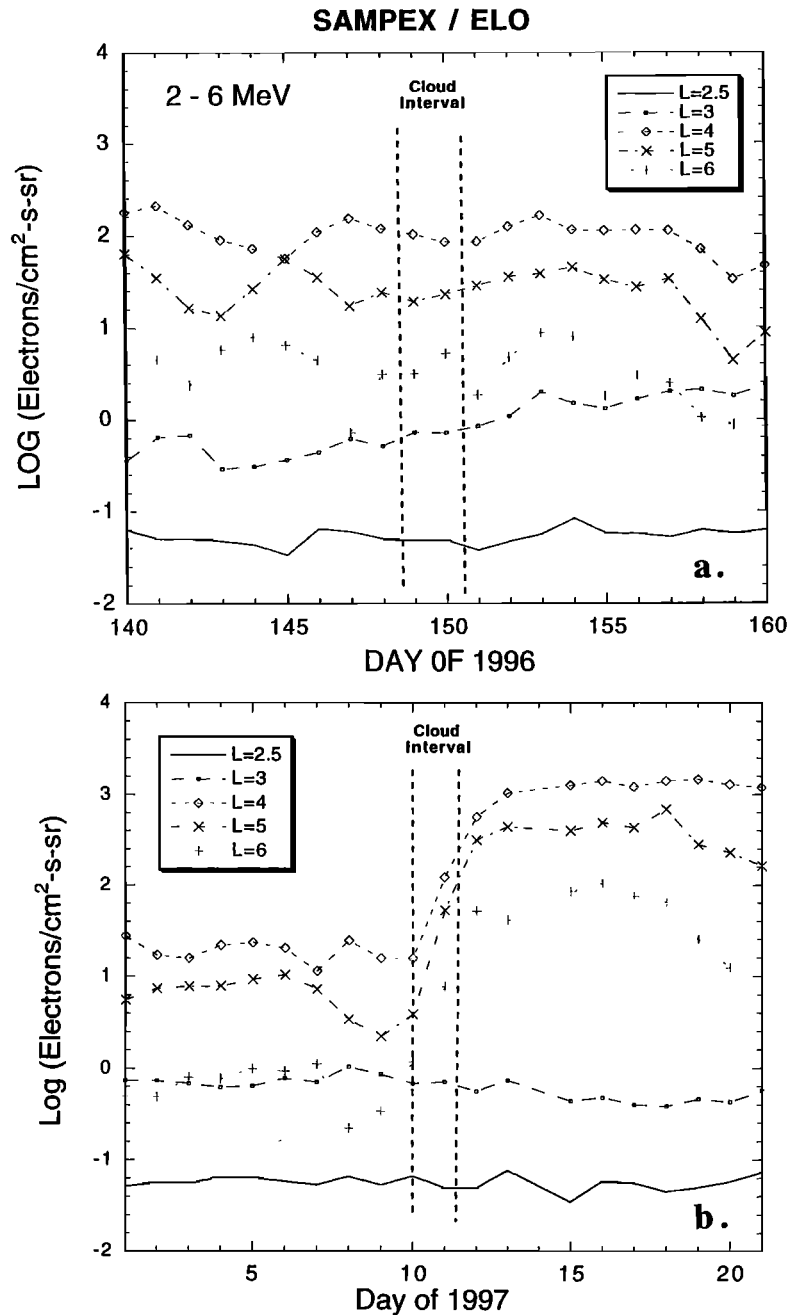
The POLAR outbound pass toward the right in Plate 3 occurred during the time (~1400 UT) that the leading portion of the magnetic cloud passed over the Earth (see Figure 3a). The IMF B_z was turning southward and substorm activity was strong. Large fluxes of relatively low energy electrons were

seen in the outer zone ($L=4\sim7$). Trapped ("pancake") pitch disturbances were indicated by the high intensities of electrons (broadly) seen at roll angles near $0°$ and $180°$. The large "loss cones" are evident for the trapped particle distributions and show up as diagonal bands of depleted flux. These flux minima trace out the local magnetic field direction, as seen by the POLAR magnetometer (data not shown here). The moderate-energy electrons seen in Plate 3 were apparently produced, in part, by the substorm activity discussed above for this case, but there was clearly a population of energetic electrons present throughout the outer zone prior to the cloud's arrival (i.e., from 0930 to ~1300 UT).

The flux versus L for various energy ranges for the relevant POLAR passes through the radiation belts can be compared as a function of time. Figure 6a shows HIST channel 10 (1.9-2.9 MeV) electron differential fluxes versus L for cuts that occurred from May 26 (~0200-1800 UT) through May 29 (~1800 UT). Each succeeding cut is offset by a factor of 10 from the previous pass in order to allow clear plotting of each profile. Each profile has the day/UT of the start of the L cut. It is evident from the data in Figure 6a that the magnetic cloud interval (1400 UT on May 27 to 1200 UT on May 29) did not change the radial flux profiles dramatically compared to the "precloud" levels (although some modest changes were seen orbit to orbit). The last cut on May 29 showed quite a drop in flux at the inner edge of the outer belt ($L \leq 3.5$).

3.2 Case 2. January 10-11, 1997

Figure 3b is analogous to Figure 3a and shows the interplanetary conditions for January 9-11, 1997. The magnetic

SAMPEX / ELO

2 - 6 MeV

Cloud
Interval

L=2.5
L=3
L=4
L=5
L=6

LOG (Electrons/cm²-s-sr)

DAY OF 1996

a.

Cloud
Interval

L=2.5
L=3
L=4
L=5
L=6

Log (Electrons/cm²-s-sr)

Day of 1997

b.

Figure 5. (a) L-sorted electron fluxes measured at low altitudes by SAMPEX instrumentation (2-6 MeV). Data are shown for days 140-159 of 1996 (May 19 to June 7). No significant electron increase was seen during the magnetic cloud interval (shown by the vertical dashed lines). (b) Similar to (Figure 5a) but for days 1-21 (January 1-21) of 1997. In this case a strong electron enhancements occurred during the cloud interval.

cloud event in this case extended from ~0100 UT on January 10 through ~0600 UT on January 11. In the central part of the cloud (~0900 - 2400 UT on January 10), the IMF magnitude was remarkably steady at B~15 nT. During this time period, B_z went from ~-15 nT (i.e., the IMF was almost exclusively southward) to ~+15 nT. Toward the end of the cloud passage, B_z was over +20 nT, and B reached exceptionally high values ($\geq$ 25 nT).

The bottom two panels of Figure 3b show that V within the cloud interval was in the range of 400-450 km/s – not

exceptionally high for solar wind bulk flow speed. However, toward the end of the cloud passage, the flow speed went up to between 500 and 600 km/s. This was a "compound" event in which the magnetic cloud was being overtaken by a recurrent high-speed solar wind stream (L. Burlaga, private communication, 1997). Thus the high-speed flows following the cloud passage were more characteristic of typical stream interaction events. Perhaps the most notable signature associated with this whole event was seen in the solar wind density profile (bottom panel): Around 0200 UT on January 11,
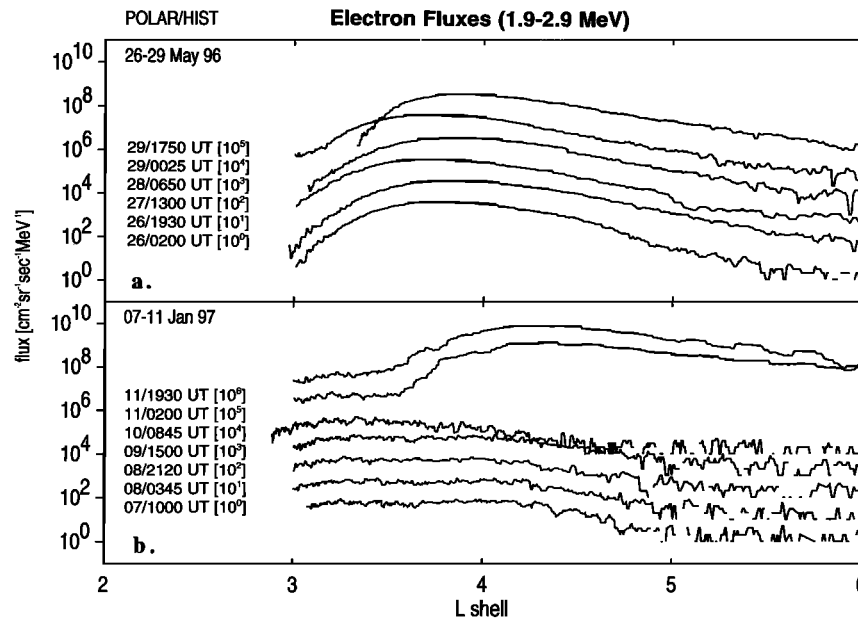
Figure 6. (top) Flux versus L value for electrons with $1.9<E\leq2.9$MeV during the period May 26-29, 1996. Data are from the POLAR/HIST sensor. Each succeeding curve is offset upward by a factor of 10 from the preceding curve. Little substantial change occurred in the sequence until the last cut on May 29. (bottom) A similar set of data for January 7-11, 1997. A large change in electron intensities for $L>3.5$ occurred between ~0900 UT on January 10 and ~0200 UT on January 11 in association with the magnetic cloud passage.

the number density briefly went up to nearly 200 cm^{-3}. This high density preceded the highest values of B noted above. Such high solar wind densities, speeds, and IMF strengths could each individually cause significant magnetospheric responses; in combination, one would expect even more pronounced effects.

Figure 4b shows some of the magnetospheric consequences of the cloud passage. The data are analogous to Figure 4a. Note that ε was much higher in this case compared to case 1. Early on January 10, ε went up to ~2×10^{12}W, and it stayed well above 10^{11}W for much of the cloud interval. Such strong energy coupling to the magnetosphere obviously drove strong geomagnetic activity. The CANOPUS AU and AL indices showed powerful enhancements through most of January 10 and AL reached nearly -1500 nT around 0900 UT on that day (off scale in Figure 4b). This strong substorm activity was accompanied by substantial ring current development, and Dst reached ~-80 nT when $|AL|$ was a maximum. Note that Dst went strongly positive at ~0100 UT on January 11 when the solar wind density spike occurred.

The bottom two panels of Figure 4b show that there was intense variability of >50 keV electron and proton fluxes at geostationary orbit during the cloud passage. These fluxes were seen to change by several orders of magnitude, in some cases, on timescales of minutes. Such highly fluctuating particle intensities are indicative of great variability in the magnetic field near geostationary orbit and are also consistent with substantial substorm acceleration of particles in the outer magnetosphere [*Reeves et al.*, 1997, and references therein].

In contrast to the May 27-29 case (where little relativistic electron acceleration apparently occurred in the outer ra-

diation belt), the January 10-11 cloud had a much more significant effect. Figure 5b shows 3 weeks (January 1-21) of 2-6 MeV electron measurements from SAMPEX. In analogy with Figure 5a, the data shown are sorted according to L (2.5 to 6). From $L=4$ to $L=6$, the electron fluxes rose quite abruptly and distinctively by at least a factor of 100 during the cloud passage interval. After the cloud passage, the flux levels at $L=4$ and $L=5$ stayed high (and nearly flat) for more than 10 days.

The nature of the relativistic electron flux change at low altitude for this case is illustrated by the global maps of $E>1$ MeV electrons from SAMPEX. Plates 2d-2f show the northern hemisphere projections for January 8-10 (in analogy with May 27-29 in Plates 2a-2c). It is seen that on January 8 and 9 there were very weak and narrow radiation belt projections at the SAMPEX (600-km) altitude. However, on January 10, with the magnetic cloud's arrival, the outer radiation zone projection was much broader and more intense. Note that the "collar" of bright red around the northern pole in Plate 2f was broader, more intense, and more azimuthally complete than for any of the May 1996 days. Hence the radiation belts became very elevated in the January case.

The abruptness and the strength of the radiation belt acceleration at high (near-equatorial) altitudes is clearly demonstrated in Figure 6b. These flux versus L profiles for the POLAR/HIST sensor (similar to Figure 6a), show the immense difference in measured peak intensity and outer belt width before, and after, the magnetic cloud reached the Earth: Prior to ~0800 UT on January 10, peak fluxes for 1.9-2.9 MeV electrons were at $3\leq L\leq4$ and were $\leq10^3$ electrons (cm^2-s-sr-MeV)$^{-1}$. By ~0200 UT on January 11, the peak intensity was at $L>4$ and the peak flux was ~5 x 10^5 electrons (cm^2-s-sr-MeV)$^{-1}$. Note also that relativistic electrons

were near counting backgrounds beyond $L \approx 5$ prior to the cloud passage but were extremely high even at $L \geq 6$ after the cloud passage.

The speed and global coherence of the electron acceleration in the January event is shown in Plate 4. The top panel shows the $E>3$ MeV electron counting rates at various L values for the SAMPEX sensors for the period January 1-30, 1997. There were essentially no detectable electrons in this energy range prior to January 10. As the magnetic cloud reached Earth, the electrons jumped up in flux at a broad range of L values ($3.5 \leq L \leq 5$) almost simultaneously. The lower panel shows line plots of POLAR/HIST, Highly-Elliptical Orbit (HEO), and LANL (geostationary orbit) data in comparable energy ranges for the same time period. The HEO spacecraft [see *Blake et al.*, 1997] is in a 60°-inclination orbit with 7 R_E apogee; it makes two cuts through the radiation belts every 12 hours. All of the measurements show similar time behavior thus emphasizing the global, coherent electron acceleration that occurred.

4. Relativistic Electron Acceleration Mechanism

As discussed by *Rostoker et al.* [1995a], large-amplitude magnetic fluctuations throughout the magnetosphere imply a global wave field in which dB/dt is large. Such an induced electric field could be effective in accelerating electrons throughout the outer zone. Moreover, this could go on concurrently and continually as long as the wave field was present. The level and duration of large-amplitude, low-frequency wave activity for the January period was strikingly greater than for the May period. This is illustrated in Figure 7 where the high-pass filtered data from several CANOPUS magnetometer stations are shown for May 27 and for January 10. The amplitudes of the field fluctuations are commonly a factor of 5 greater in the January case. The largest amplitude waves seen by CANOPUS on January 10 occurred between ~1000 and ~1130 UT. This was the approximate time that SAMPEX and POLAR saw the relativistic electrons suddenly increase in flux (see *Reeves et al.*, 1998).

A significant difference between the May 1996 and the January 1997 cloud periods was the level of substorm activity produced within the magnetosphere as the leading edges of the magnetic clouds passed the Earth. This is clearly shown by the very different levels of AL in the two cases. As also shown by Figures 4a and 4b, the substantially different substorm activity levels changed very much the intensities and time variabilities of low-to-moderate energy electrons at geostationary orbit. The available quantity of such electrons in the outer magnetosphere could play an important role in determining the ultimate flux of relativistic electrons that are produced. In the picture presented by *Baker et al.* [1997b], there is a two-step process: First, substorm activity generates a low-energy "seed population" and then, in a second step, some portion of these substorm generated electrons are further energized (see Figure 2). The new and compelling evidence from the present analysis is that the second step of the acceleration is closely associated with large amplitude, low-frequency waves. As also suggested by the work of *Blake et al.* [1997], all the solar wind features must be in play (large, southward IMF and relatively high speed solar wind flow) to get relativistic electron acceleration.

5. Discussion

We have shown in this paper two magnetic clouds that, superficially, seem quite similar. However, when examined in detail, the January 1997 cloud event was much more effective at accelerating high-energy electrons. The January event led to much stronger substorm activity and ring current development and it also produced much stronger global fluctuations in the geomagnetic field. These fluctuations in B would imply a large-scale induced electric field which could accelerate further the electrons produced initially by the strong substorm events that occurred as the leading edge of the magnetic cloud passed the Earth. However, the details of how such in situ acceleration can occur have still to be worked out.

Figure 8 shows a schematic summary of our inferences concerning the acceleration process. For the January 1997 period, the radiation belts were very weak prior to the magnetic cloud arrival. The relativistic flux levels were low and only a small range of L values was populated substantially. When the January magnetic cloud struck the magnetosphere, there was strong substorm activity associated with the leading edge (in which the IMF was strongly southward). As shown in Figure 8b, a high-density population of magnetospheric electrons was produced by the substorm activity and this population rapidly diffused inward and was further accelerated by the strong induced electric fields of the low-frequency waves. Finally, and on quite a short timescale, the entire magnetosphere was filled with high-energy electrons.

The scenario shown in Figure 8 is not fundamentally different from the one which has previously been discussed for recurrent storms associated with high-speed solar wind streams (see Figure 2). However, the January CME event produced higher-energy electrons much more quickly than typically seen in stream-associated events. This suggests that the January cloud somehow was more efficient at relativistic electron production than are normal high-speed streams.

As a first step to analyze the efficiency question, one can easily integrate the energy input (ε) parameter discussed above for the two cloud cases. Doing this for the entire cloud interval on May 27-29, one gets $\int \varepsilon dt \sim 2.0 \times 10^{16}$J. Limiting the calculation to only the southward IMF period, this integral equals $\sim 1.5 \times 10^{16}$J. For the January case, the integral for the entire cloud is $\int \varepsilon dt \sim 7.0 \times 10^{16}$J, while for the southward IMF interval the integral is $\sim 5.5 \times 10^{16}$J for January 10. Thus, perhaps a bit surprisingly, the January cloud was only a factor of about 3 to 4 "stronger" in total electromagnetic energy input than the May cloud.

An obvious further issue concerning the outer zone electron population is what fraction of the total magnetospheric input energy gets converted to relativistic electrons. One can make a rough calculation of this "efficiency factor" as follows: Let us assume for calculational convenience that the outer zone is actually a torus of circular cross section. Then the cross-sectional area is given by $A_T = \pi r_T^2$, where r_T is the torus (minor) radius. The volume (V_T) of this torus is roughly $2\pi r_B A_T$, where r_B is the central (major) torus radial dimension. Thus the volume of the assumed belt of particles is $V_T = 2\pi^2 r_T^2 r_B$.

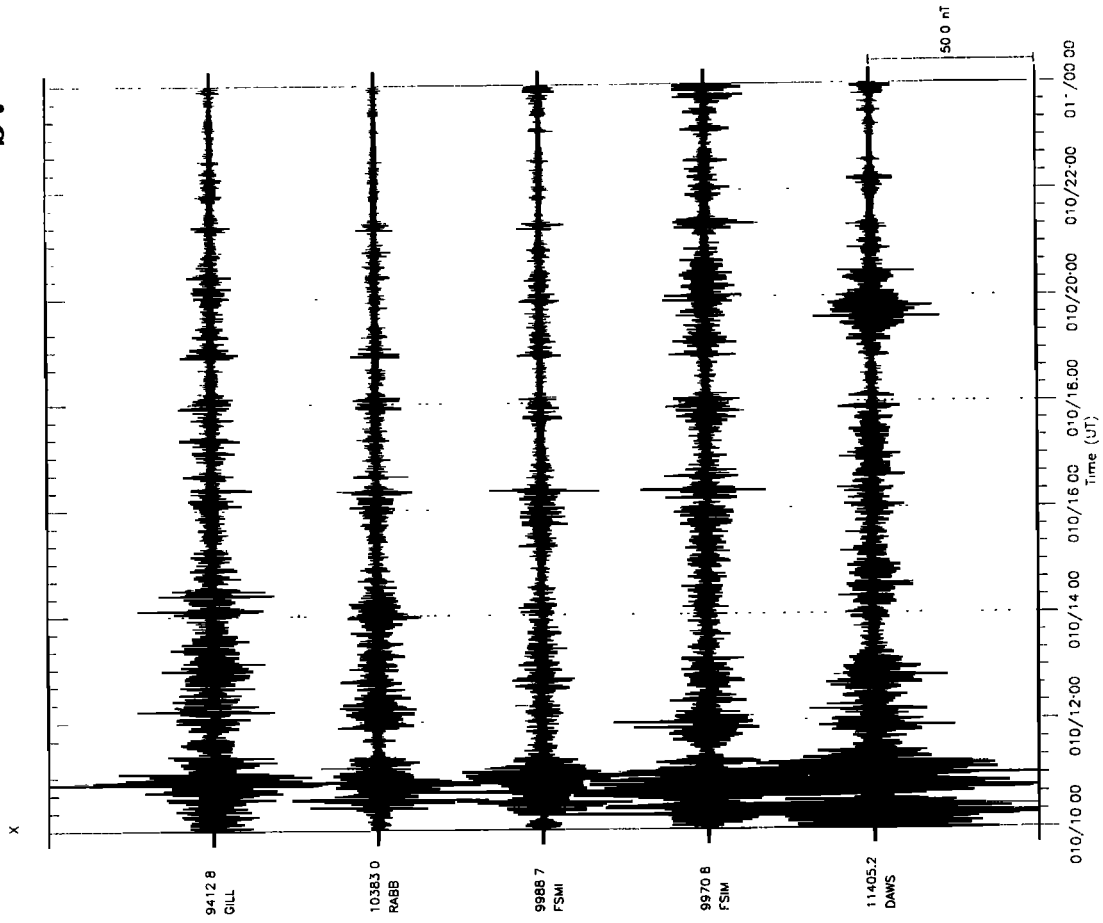The geometrical quantities for the January cloud event can be estimated from the available particle measurements. Be-
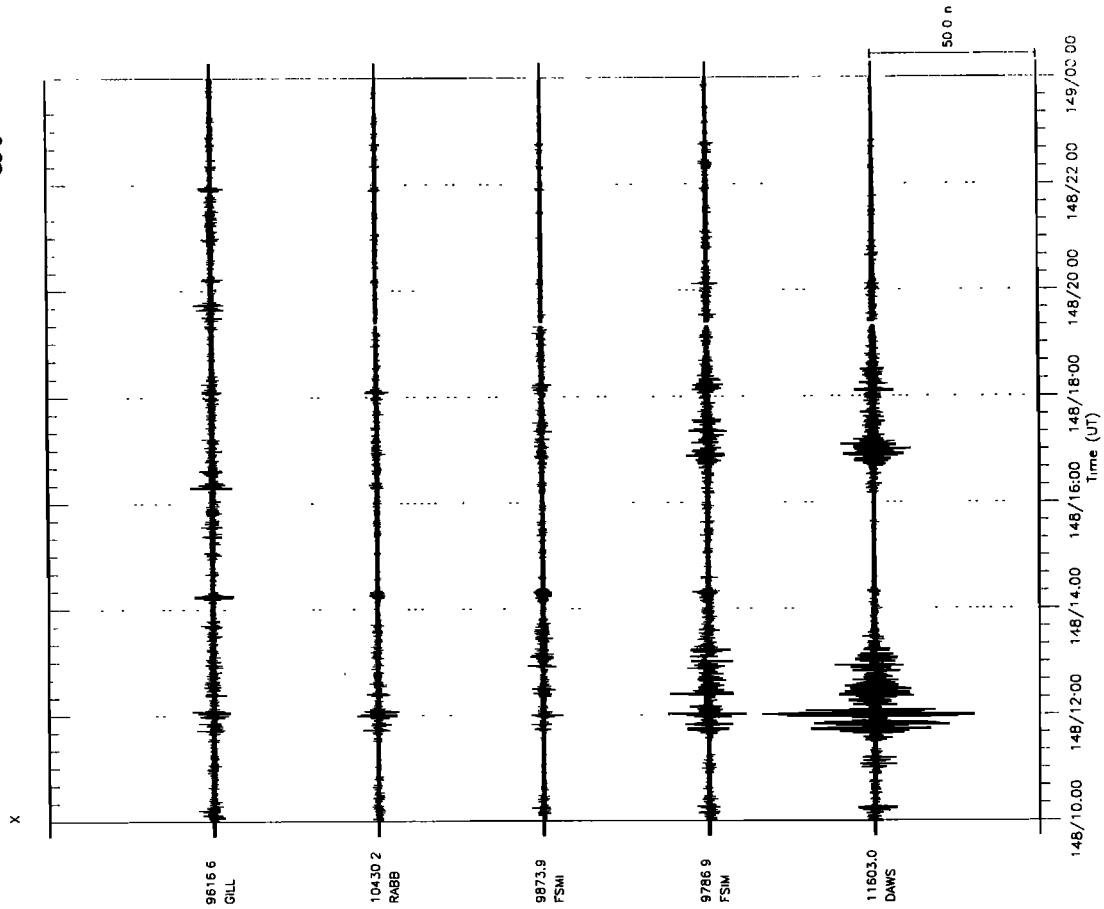
Figure 7. A comparison of low-frequency wave properties measured at various CANOPUS ground stations for May 27, 1996, and January 10, 1997. Much larger wave amplitudes were seen at all stations in the January case: These waves may have played a key role in subsequent electron acceleration.

a.

Substorm Electrons

Outer Zone Electrons

b.

Acceleration via dB/dt Effects

Outer Zone

c.

Relativistic Electrons Filling Outer Zone

Outer Zone
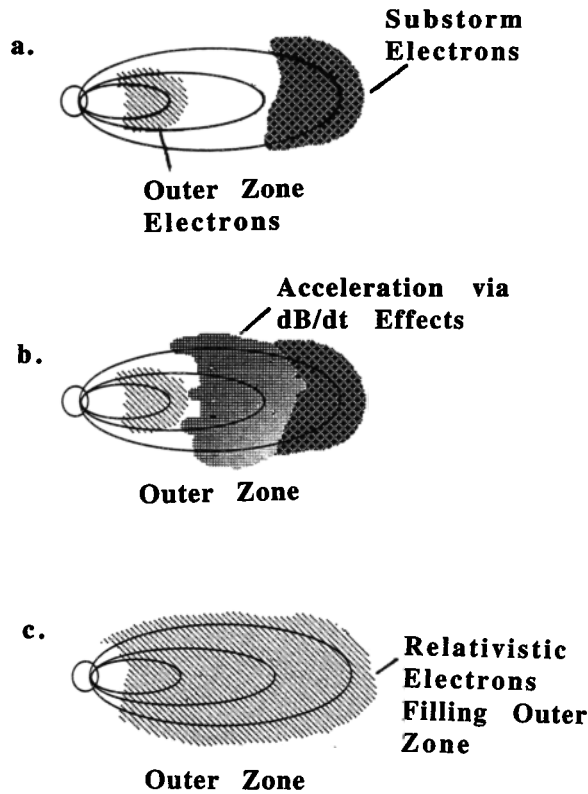
Figure 8. A schematic summary of the electron acceleration and redistribution which occurred during the January 1997 CME event.

fore the cloud passage on January 8 and 9 (see Figure 6b), one gets r_T=0.75 R_E and r_B=3.75 R_E. This gives

$$V_T=1.08 \times 10^{28} \text{ cm}^3.$$

After the cloud passage (i.e., after midday on January 10), it is estimated that $r_T = 2.0 \, R_E$ and $r_B = 5.0 \, R_E$. This gives

$$V_T=1.02 \times 10^{29} \text{ cm}^3$$

after the cloud has interacted with the magnetosphere.

Taking the relativistic belt electrons to be those with E>0.5 MeV, one can use POLAR/HIST and SAMPEX to estimate the average particle fluxes in the torus region. Using the measured electrons at various energies to estimate the integral energy spectrum as $J(>E) = \kappa E^{-2}$, an average flux for E>0.5 MeV is calculated to be

$$J(>0.5 \text{ MeV}) = 2.4 \times 10^5 \text{ (cm}^2 \text{ -s)}^{-1}$$

on January 9. By January 11 we estimate a factor of $\geq$100 increase to

$$J(>0.5 \text{ MeV}) = 3 \times 10^7 \text{ (cm}^2 \text{ -s)}^{-1}.$$

Since the electrons are moving at $v \sim c$, density can be estimated from

$$n \sim J/c$$

and $<n>_1$ = 8×10^{-6} cm^{-3} before the cloud passage and $<n>_2$=10^{-3} after the cloud passage.

Using these average relativistic electron number densities, along with the torus volumes computed previously, the number of electrons in the radiation belts is estimated from

$$N_B=V_T<n>$$

with N_B =8.6$\times 10^{22}$ electrons before the cloud passage and N_B=1.0$\times 10^{26}$ after the cloud passage. Taking an average electron energy for this population of ~1 MeV (=1.6$\times 10^{-13}$J),

$$W_1=1.4 \times 10^{10} \text{J}$$

is the relativistic electron energy content of the outer zone before the cloud and

$$W_2=1.6 \times 10^{13} \text{J}$$

after the cloud passage.

Finally, to compute the relativistic electron efficiency factor (η_R), we use

$$\eta_R = \left(\frac{W_2 - W_1}{\int \varepsilon dt} \right).$$

Taking the integral of ε as ~5$\times 10^{16}$J from above, this works out to be η_R ~3.2 x 10^{-4}. Hence the electron acceleration efficiency was ~ 0.03% in the January case. Notably, of course, the May cloud event must have had a very much lower (nearly negligible) acceleration efficiency.

5. Summary and Conclusions

This paper has compared and contrasted two magnetic cloud events observed by a large number of ISTP and affiliated spacecraft. It has also used a variety of ground-based data sets to assess the nature of the cloud's interactions with the magnetosphere. It was found that the May 1996 magnetic cloud was not effective in accelerating high-energy electrons in the outer radiation zone. On the other hand, the magnetic cloud event in early January 1997 was much more effective in producing large flux enhancements of relativistic electrons throughout the outer zone ($L \geq 3.5$). We observed such large differences in "geoeffectiveness" despite the superficial similarity of the solar wind/IMF properties within the two clouds.

We conclude that the January cloud had the requisite features of strong southward IMF and high enough solar wind speed to accelerate high-energy electrons. The high-density spike following the cloud may also have played an important role for the later, long-duration enhancement in January 1997. The combination of interplanetary drivers is generally the same as those which result in effective electron acceleration during high-speed solar wind stream events. Thus any solar disturbance that produces suitable solar wind "input" conditions at 1 AU , whether from coronal holes, or from CMEs, can be very effective at enhancing the Earth's radiation belts. In particular, events that drive strong, low-frequency wave activity clearly can accelerate electrons with

remarkable speed and efficiency [*Rostoker et al.,* 1997]. This suggests that electron acceleration to high energies might have similar causes in other (e.g., solar or astrophysical) contexts.

References

Acuña, M.H., K.W. Ogilvie, D.N. Baker, S.A. Curtis, D.H. Fairfield, and W.H. Mish, The global geospace science program and its investigations, in *The Global Geospace Mission,* edited by C.T. Russell, p. 5, Kluwer Acad., Norwell, Mass., 1995.

Baker, D.N., Solar wind-magnetosphere drivers of space weather, *J. Atmos. Terr. Phys., 58,* 1509, 1996.

Baker, D.N., P.R. Higbie, E.W. Hones Jr., and R.D. Belian, High-resolution energetic particle measurements at 6.6 R_E, 3, Low-energy electron anisotropies and short-term substorm predictions, *J. Geophys. Res., 83,* 4863, 1978.

Baker, D.N., J.B. Blake, R.W. Kelbesadel, and P.R. Higbie, Highly relativistic electrons in the earth's outer magnetosphere, 1, Lifetimes and temporal history 1979-1984, *J. Geophys. Res., 91,* 4265, 1986.

Baker, D.N., et al., Relativistic electron acceleration and decay time scales in the inner and outer radiation belts: SAMPEX, *Geophys. Res., Lett., 21,* 409, 1994.

Baker, D.N., et al., An assessment of space environmental conditions during the recent Anik E1 spacecraft operational failure, *ISTP Newsl., 6,* (2), 8-29, June, 1996.

Baker, D.N., et al., Recurrent geomagnetic storms and relativistic electron enhancements in the outer magnetosphere: ISTP coordinated measurements, *J. Geophys. Res., 102,* 14,141, 1997a.

Baker, D.N., X. Li, J.B. Blake, and S. Kanekal, Strong electron acceleration in the Earth's magnetosphere, *Adv. Space Sci.,* in press, 1997b.

Blake, J.B., et al., CEPPAD, Comprehensive Energetic Particle and Pitch Angle Distribution Experiment on POLAR, *Space Sci. Rev., 71,* 531, 1995.

Blake, J.B., D.N. Baker, N. Turner, K.W. Ogilvie, and R.P. Lepping, Correlation of changes in the outer-zone relativistic-electron population with upstream solar wind and magnetic field measurements, *Geophys. Res. Lett., 24,* 927, 1997.

Burlaga, L.F., *Interplanetary Magnetohydrodynamics,* Chap. 6, Oxford Univ. Press, New York, 1995.

Feldman, W.C., et al., Long-term variations of selected solar wind properties: IMP 6, 7, and 8 results, *J. Geophys. Res., 83,* 2177, 1978.

Gosling, J.T., The solar flare myth, *J. Geophys. Res., 98,* 18,937-18,949, 1993.

Hruska, A., and J. Hruska, Solar wind modulation of the auroral zone geomagnetic activity when the interplanetary magnetic field has a strong northward component, *J. Geophys. Res., 94,* 5479, 1989.

Kahler, S.W., Solar flares and coronal mass ejections, *Annu. Rev. Astron. Astrophys., 30,* 113, 1992.

Lepping, R.P., et al., The WIND magnetic field investigation, *Space Sci. Rev., 71,* 207-220, 1995.

Li, X., et al., Are energetic electrons in the solar wind the source of the outer radiation belt? *Geophys. Res. Lett., 24,* 923, 1997a.

Li, X., et al., Multi-satellite observations of the outer zone electron variation during the 3-4 November 1993 magnetic storm, *J. Geophys. Res., 102,* 14,123, 1997b.

Mayaud, P.N., *Derivation, Meaning, and Use of Geomagnetic Indices,* AGU, Washington, D.C., 1980.

Nishida, A., IMF control of the Earth's magnetosphere, *Space Sci. Rev., 34,* 185, 1983.

Ogilvie, K.W., et al., SWE, A comprehensive plasma instrument for the WIND spacecraft, *Space Sci. Rev., 71,* 55-77, 1995.

Paulikas, G.A., and J.B. Blake, Effects of the solar wind on magnetospheric dynamics: Energetic electrons at the synchronous orbit, in *Quantitative Modeling of Magnetospheric Processes, Geophys. Monogr. Ser.,* vol. 21, edited by W. P. Olsen, p. 180, AGU, Washington, D.C., 1979.

Perreault, P., and S.-I. Akasofu, A study of geomagnetic storms, *Geophys. J. R. Astron. Soc., 54,* 547, 1978.

Reeves, G.D., et al., The relativistic electron response at geosynchronous orbit during the January 1997 magnetic storm, *J. Geophys. Res.,* in press, 1998.

Rostoker, G., S. Skone, and D.N. Baker, Correlated measurements of relativistic electrons at SAMPEX with ULF measurements from the CANOPUS magnetometer chain, paper presented at IUGG Meeting, Boulder, Colo., 1995a.

Rostoker, G., et al., CANOPUS – A ground-based instrument array for remote sensing the high latitude ionosphere during the ISTP/GGS program, *Space Sci. Rev., 71,* 743, 1995b.

Rostoker, G., S. Skone, and D.N. Baker, On the origin of relativistic electrons in the magnetosphere, Geophys. Res. Lett., submitted, 1997.

Williams, D.J., A 27-day periodicity in outer zone trapped electron intensities, *J. Geophys. Res., 71,* 1815, 1966.

D.N. Baker and X. Li, Laboratory for Atmospheric and Space Physics, University of Colorado, Boulder, CO 80303.

J.B. Blake and R.S. Selesnick, The Aerospace Corporation, Space and Environment Technology Center, P.O. Box 92957, Los Angeles, CA 90009.

M.G. Henderson and G.D. Reeves, Los Alamos National Laboratory, Los Alamos, NM 87545.

S.G. Kanekal, NASA Goddard Space Flight Center, Greenbelt, MD 20771.

T.I. Pulkkinen, Finnish Meteorological Institute, Helsinki, Finland.

G. Rostoker, Department of Physics, University of Alberta, Edmonton, Canada T6G 2J1.

H.E. Spence, Center for Space Physics, Boston University, Boston, MA 02215.